Automatic Measurement of Spine Curvature on 3-D Ultrasound Volume Projection Image with Phase Features

Guang-Quan Zhou, Wei-Wei Jiang, Ka-Lee Lai, Yong-ping Zheng*, *Senior Member, IEEE*

***Abstract*—This paper presents an automated measurement of spine curvature by using prior knowledge on vertebral anatomical structures in ultrasound volume projection imaging (VPI). This method can be used in scoliosis assessment with free-hand 3-D ultrasound imaging. It is based on the extraction of bony features from VPI images using a newly proposed two-fold thresholding strategy, with information of the symmetric and asymmetric measures obtained from phase congruency. The spinous column profile is detected from the segmented bony regions, and it is further used to extract a curve representing spine profile. The spine curvature is then automatically calculated according to the inflection points along the curve. The algorithm was evaluated on volunteers with different severity of scoliosis. The results obtained using the newly developed method had a good linear correlation with those by the manual method ($r \geq 0.90$, $p < 0.001$) and X-ray Cobb's method ($r = 0.83$, $p < 0.001$). The bigger variations observed in the manual measurement also implied that the automatic method is more reliable. The proposed method can be a promising approach for facilitating the applications of 3-D ultrasound imaging in diagnosis, treatment, and screening of scoliosis.**

***Index Terms*—scoliosis; Cobb angle; 3-D ultrasound; phase congruency; thresholding; volume projection imaging**

I. Introduction

Scoliosis is a 3-D spinal disorder characterized by an angle of spine curvature larger than 10° in the coronal plane [1]. It is the most common medical condition affecting the adolescent population [2, 3]. The overall prevalence of adolescent idiopathic scoliosis (AIS) is 0.47–5.2 % of the population [3]. It is particularly concerned with the high rate of curve progression of early-onset scoliosis during the adolescent years. The Cobb angle, the spine curvature angle derived using Cobb's method on standing radiograph, has been widely used as a gold standard in scoliosis diagnosis [4]. The X-ray examinations are essential for early screening of scoliosis and monitoring curve progression [2, 5]. A 5° of increase or more between Cobb angles of two follow-up radiographs indicates a curvature progression [6]. However, frequent X-ray examinations would have harmful effects on human body, especially for children. Exposure to multiple diagnostic radiographic examinations over their growth period may increase the risk of cancer development in the AIS patients [7-10]. Moreover, the measurement accuracy of Cobb angle is dependent on the awareness and practice of the observer and the quality of images. The intra-observer and inter-observer variations of Cobb angle measurement have been reported to be 3 - 5° and 6 - 9°, respectively [6, 11, 12], restricting the application of radiograph in monitoring curve progression. Recently, a slot scanning X-ray system (EOS Imaging, Paris, France) has been developed to capture X-ray images using low radiation dose [13, 14]. This system also allows 3-D imaging using a special software program named SterEOS®, by combing anatomical information obtained along two orthogonal planes, The EOS system is relatively expensive for both the device and its operation [15, 16]. Its accessibility will therefore not be high in the foreseeable future. In addition, as it requires 10 to 20 minutes to manually identify anatomical landmarks in both frontal and sagittal views [15], which is time-consuming for 3-D imaging.

Magnetic resonance imaging (MRI) has been used to identify the bony features for the study of scoliotic spine due to its high resolution with 3-D information. However, subjects have to undergo the examinations in a supine posture, which is different from the measurements taken in widespread standing posture [6]. It is also time-consuming and expensive for performing MRI examinations. Moreover, although some automatic and semi-automatic methods have been advanced to segment vertebrae and spinal cord from MRI images [17], there is little report on scoliosis measurements using these methods [18].

Ultrasound imaging is a real-time and cost-effective as well as radiation-free imaging technique. Although 2-D ultrasound lacks the ability to view complex 3-D spine structure, it has been proposed to measure the vertebrae rotation in idiopathic scoliosis [19, 20]. Recently, some free-hand 3-D ultrasound

Asterisk indicates corresponding author

Guang-Quan Zhou is with State Key Laboratory of Bioelectronics, School of Biological Science and Medical Engineering, Southeast University, Nanjing, China, and is also with the Interdisciplinary Division of Biomedical Engineering, The Hong Kong Polytechnic University, Hong Kong, China (e-mail: guangquan.zhou@seu.edu.cn).

Wei-Wei Jiang is with the Interdisciplinary Division of Biomedical Engineering, The Hong Kong Polytechnic University, Hong Kong, China.

Ka-Lee Lai is with the Interdisciplinary Division of Biomedical Engineering, The Hong Kong Polytechnic University, Hong Kong, China (e-mail: kelly.lai@polyu.edu.hk).

*Yong-ping Zheng is with the Interdisciplinary Division of Biomedical Engineering, The Hong Kong Polytechnic University, Hong Kong, China (e-mail: ypzheng@ieee.org).

systems, combining B-mode ultrasound with position sensors, have been developed to overcome the limitations of 2-D viewing [21-31]. The feasibility of using body landmarks in B-mode ultrasound images acquired with continuous scanning approach, including laminae and transverse process, to assess spine curvature has been demonstrated in *in vitro* experiments [21-25]. However, this method is tedious and subjective, since each required body landmark has to be manually identified in dozens of ultrasound images [22-24]. Moreover, the performance of *in vivo* measurements using body landmarks became apparently worse than that of *in vitro* measurements, especially for subjects with high body mass index (BMI) [26].

Alternatively, 3-D volume reconstruction and visualization can be employed to reveal pathology obscured in 2-D viewing by constructing 3-D data from a series of 2-D ultrasound images [32]. The feasibility of 3-D volume reconstruction for imaging complex 3-D spine structure was firstly demonstrated using nearest neighbor (NN) method [27]. Recently, the visualization of spine anatomy has been successfully acquired from 3-D volume data using different visualization methods, such as maximum intensity projection [28] and volume projection imaging (VPI) [29]. Chen, et al. [28] used the center of lamina as landmarks to assess the spine curvature on the coronal visualization of spine anatomy. On the other hand, the spinous column profile was exploited as landmarks to perceive the spine curve in the spine VPI image (VPI-SP) [29]. These methods can provide reliable spine curvature measurements with performance comparable to that of X-ray Cobb's method *in vivo* [29, 30], suggesting their feasibility and potential in the diagnosis and treatment of scoliosis. However, the measurements are still influenced by the knowledge and experience of observers. The intra-observer variation of angle measurement for the same image can be 2-3° [29, 30], though it is much smaller than that of X-ray Cobb's method [6, 11, 12]. In addition, measurement time highly depends on the observer experience and the detectability of the inflection points, varying from about 20 to 60 seconds per VPI image. To fully realize the 3-D ultrasound VPI method for the mass screening, diagnosis, and follow-up observation of scoliosis, an automatic method for measuring spine curvature is clearly necessary.

In previous research by our group [29, 33], the spinous column profile was utilized to estimate the spine curvature angle in VPI images. As illustrated in Fig. 1, the line portions denoting the location of the inflection points were required to be manually identified over the spinous column profile for calculating the spine curvature angle using VPI-SP method [29]. Our previous work [33] also explored the automatic measurements using the spinous column profile segmented by Otsu method [34]. Fig. 1 shows that the spinous column profile is characterized by a 1-D valley-like curve in each row. The "valley bottom" is defined as the location of the lowest point of this valley-like curve (Fig. 1b), i.e. the pixel with the smallest intensity within the spinous column region. This valley bottom was then employed to locate spine curve in VPI images, which was approximated with a high-order polynomial regression curve fitted to the intensity distribution of each row in VPI image. The curvature was finally calculated by fitting a 6th order

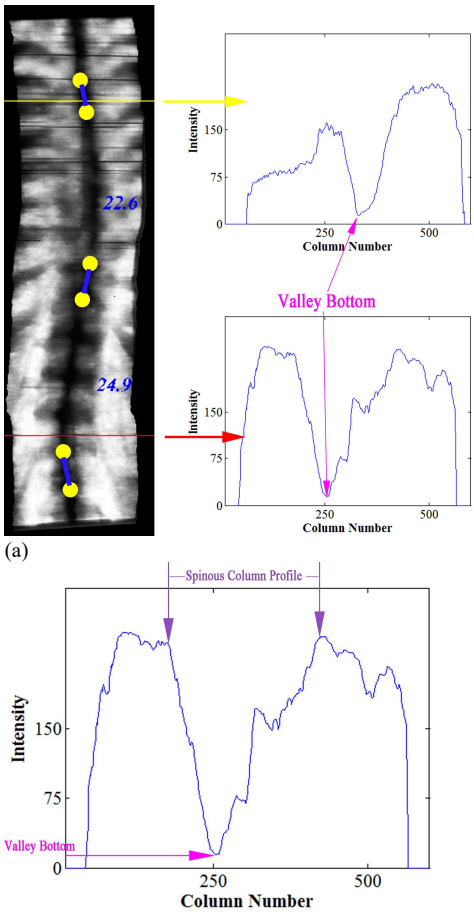

Fig. 1. An example of spine curvature measurement using VPI-SP method on the spine VPI image (image width: 12.3cm, height: 42.9cm): (a) The results using manual VPI-SP method (b) The definition of valley bottom in spinous column profile. Blue lines with yellow dots are the manually identified lines containing inflection points in VPI-SP method. The numbers in blue text represent the angle between two adjacent drawn lines. Scanline profiles of the two (yellow and red) horizontal lines represent valley-like intensity distribution (row numbers are 400 and 1800) due to the symmetry of vertebral anatomical structures. The text and arrows in purple and pink indicate the spinous column profile and its corresponding valley bottom, respectively.

polynomial curve to the estimated points. Although this method was simple and fast, common thresholding techniques, such as Otsu method, cannot always get a satisfying segmentation of spinous column profile from the VPI image that has no distinct valley point in the histogram, degrading the measurement accuracy of spine curvature. Additionally, the estimated points might not be accurate without using the actual valley bottom in spinous column profile.

In this study, a novel automatic method was presented to estimate the spine curvature in VPI images. We significantly extended our previous work by utilizing prior knowledge on vertebral anatomical structure, such as its symmetry, to segment the spinous column profile and measure the spine curvature. The spine VPI image was first preprocessed with the phase congruency to measure the symmetric and asymmetric features. Then a newly developed two-fold thresholding strategy was applied to segment bony features from the preprocessed data, enabling the detection of spinous column profile and its corresponding valley bottom. Similar to the manual VPI-SP method proposed in [29], the inflection points of curve were

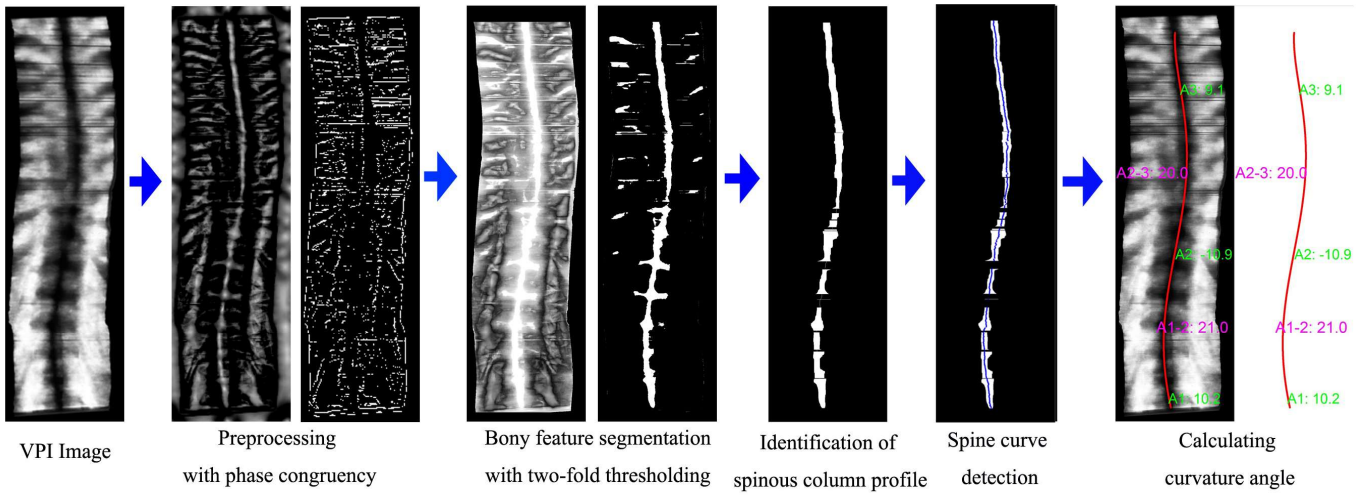

Fig. 2. Flow diagram of the proposed automatic algorithm for the spine curvature measurement. The blue line represents the valley bottom in spinous column profile, and red curve is the estimated spine curve with 6th order polynomial fitting to these valley bottoms.

finally employed to calculate the spine curvature angle. This method can essentially realize the assessment of scoliosis using 3-D ultrasound imaging by overcoming the limitations in manual measurements. The performance of the proposed method was evaluated on spine VPI images among subjects with different spine curvature angles.

The paper is organized as follows. A detailed description of the automatic method is given in Section II. *In vivo* experiments are presented to demonstrate the performance of the new automatic method in Section III and Section IV. Finally, Section V compares and discusses the tested results, and Section VI concludes the proposed work.

II. Methods

The flow diagram of the proposed method is illustrated in Fig. 2. The proposed automatic method for spine curve detection consists of preprocessing with phase congruency, bony feature segmentation, identification of spinous column profile, and finally spine curve detection. In preprocessing, the symmetric and asymmetric features were measured using phase congruency, contributing to the detection of spine region and enhancement of bony features. Bony features including transverse processes and spinous processes were separated from the VPI image using a newly developed two-fold thresholding strategy. The spinous column profile was then extracted from the bony features using prior knowledge on its arrangement in spine VPI images. Finally, the inflection points of spine curve, which were determined by using a polynomial curve fitting to the valley bottom in spinous column profile, were used for calculating curvature angle.

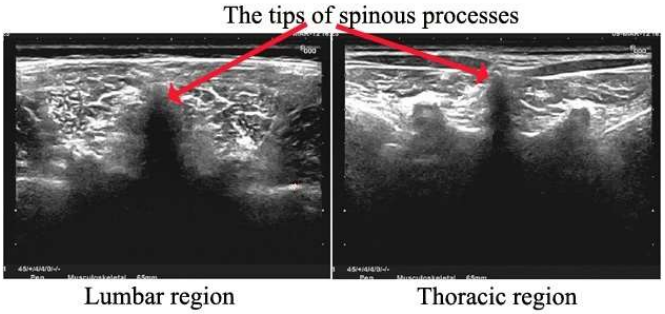

Fig. 3. The tips of spinous processes in the cross-section B-mode ultrasound images.

A. Preprocessing with Phase Congruency

In this study, 2-D ultrasound images with corresponding spatial information were used to reconstruct and visualize the 3-D spine anatomy using the VPI method introduced in [29]. As shown in Fig. 3, vertebrae with spinous processes at their body centers cause strong reflections of ultrasound wave, resulting in symmetric bony shadows in 2-D ultrasound images of lumbar region and thoracic region. The shadow generated by spinous processes was also observed to be closer to the skin surface in comparison with other bony shadows, such as transverse processes and vertebral bodies. The spinous column profile, the valley-like shadow curve lying nearby the midline of VPI image, was therefore produced due to the symmetry of vertebral anatomical structures when using the average blending function for rendering the spine anatomy [29]. The spine curvature can then be estimated by fitting a polynomial curve along the tips of spinous processes corresponding to the valley bottom of the spinous column profile. However, in our previous research [33], the spinous column profile and its corresponding valley bottom were only approximated using the common thresholding techniques and the minimum of polynomial regression curve, respectively. Hence, that method ignored or hardly used the aforementioned anatomical information about symmetric features, which deteriorated its measurement accuracy.

In VPI images, the spinous column profile depicts a 1-D valley-like curve in each row, representing an axis of local symmetry (Fig. 1). As the Fourier series at points of symmetry is either at minima or maxima of their cycle, symmetry and asymmetry in image intensity can be extracted using phase congruency [35]. It is well-known that phase congruency is an illumination and contrast invariant measure of feature significance based on the local-energy model [36]. Under the assumption that features are perceived at points where Fourier components of the signal are maximally in phase, phase

congruency can detect a wide range of feature type, including step edges, line and roof edges, and Mach bands, from the Fourier analysis. After the publication of the phase congruency method [35], it has been investigated extensively to construct symmetry descriptors for the ridge-like bone surface localization [37-41], and asymmetry descriptors for ramp-like cardiac border enhancement [42] in ultrasound images. In this work, we proposed to use the phase congruency as a sensitive feature for the detection of valley-like spinous column profile in VPI images.

Different practical approaches have been proposed to calculate the phase congruency using a quadrature pairs of filters [43, 44]. A common choice is the method using log Gabor wavelet that achieved good feature localization and noise compensation [43]. By taking the responses of log Gabor wavelet over multiple scales and orientations, the symmetric phase measure at each point in the image can be calculated according to the following equation [43]:

$$PS(x,y) = \frac{\sum_r \sum_s W(x,y)\lfloor A_{rs}(x,y)\lfloor |e_{rs}(x,y)| - |o_{rs}(x,y)| \rfloor - T_r \rfloor}{\sum_r \sum_s A_{os}(x,y) + \varepsilon} \quad (1)$$

and the asymmetry phase measure is given by

$$PAS(x,y) = \frac{\sum_r \sum_s W(x,y)\lfloor A_{rs}(x,y)\lfloor |o_{rs}(x,y)| - |e_{rs}(x,y)| \rfloor - T_r \rfloor}{\sum_r \sum_s A_{os}(x,y) + \varepsilon} \quad (2)$$

where $e_{rs}(x,y)$ is the even symmetric part and $o_{rs}(x,y)$ is the odd symmetric part of the filter at orientation r and scale s. At a point of symmetry, the absolute value of e_{rs} will approach 1 and the absolute value of o_{rs} is near 0, and vice versa. ε is a small real number to avoid division by zero, T_r is the noise threshold, and $\lfloor \cdot \rfloor$ denotes the operation: $\lfloor z \rfloor = z$ if $z > 0$; otherwise $\lfloor z \rfloor = 0$. $W(x, y)$ is the weighting factor based on frequency spread that reduces phase congruency at locations with a narrow frequency component. $A_{rs}(x,y)$ is the amplitude of wavelet response with a given scale and orientation at point (x, y).

These two phase measures were applied as a preprocessing step for perceiving and enhancing the symmetric or asymmetric features in our approach. The parameters used in computing phase congruency, such as $W(x, y)$, $A_{rs}(x,y)$, and T_r, were based on those presented in [43]. Fig. 4 presents an example of an original image and its corresponding symmetry and asymmetry phase maps.

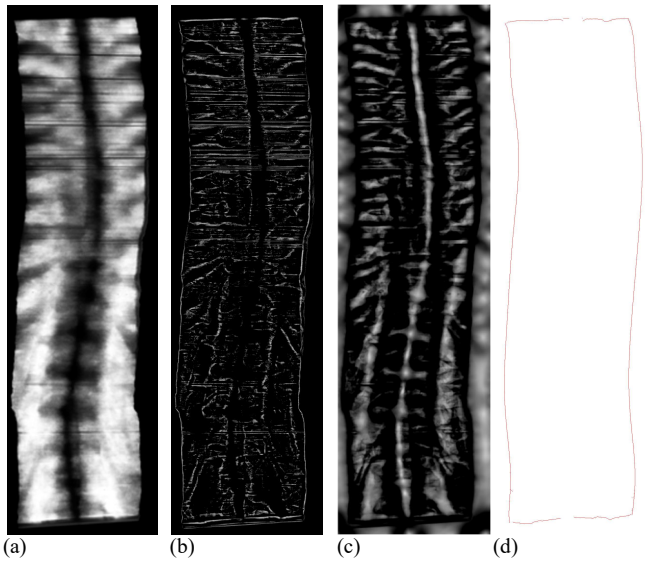

(a) (b) (c) (d)

Fig. 4. An example showing the symmetry and asymmetry phase measure: (a) Original spine VPI image (image width: 12.3cm, height: 42.9cm); (b) The asymmetry phase of the image; (c) The symmetry phase of the image; (d) Smoothed lateral border lines of spine region.

B. Bony Feature Segmentation

As narrow-band non-planar volume rendering and average blending function were used to generate the spine VPI image in [29], the foreground spine region in VPI images contained anatomy information from two sources, soft tissues and bony features. Hence, three regions, background, soft tissues, and bony features, could be readily observed in the spine VPI image (Fig. 4a). Image segmentation is the process to classify all pixels into different salient image regions, and thresholding is the easiest method for segmentation by calculating the optimum threshold from its gray level intensity (histogram) [45]. Instead of using multilevel thresholding methods to separate bony features from the image [46, 47], we developed a two-fold thresholding strategy using phase map to derive spine region and bony features, respectively.

The asymmetry phase measure provides a good measure of asymmetric image features such as step and ramp-like edges. As shown in Fig. 4b, the intensity of asymmetry phase is quite distinct from its background, which can be used to determine the contours of spine region. The Otsu method [34] was employed to calculate the global threshold T_{Otsu} on asymmetry phase map for identifying the boundary of foreground spine region. Let $PAS(x,y)$ denote the asymmetry phase measure at pixel (x,y), $x = 1, \cdots, N; y = 1, \cdots, M$. The contour of spine

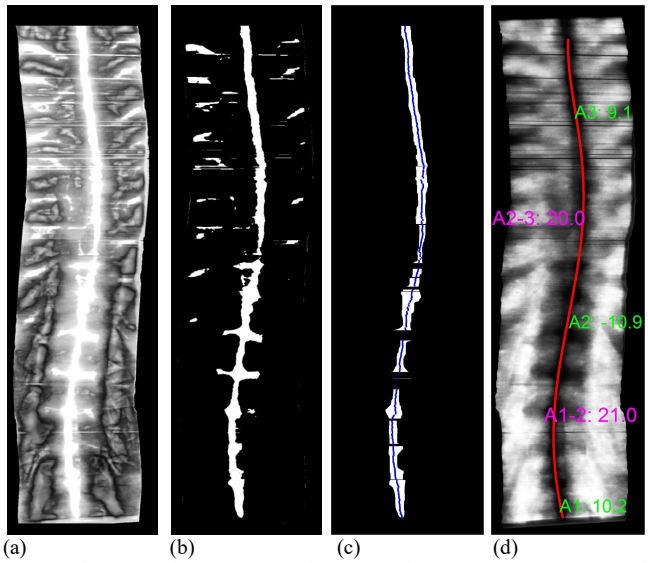

(a) (b) (c) (d)

Fig. 5. The curve detection from the image shown in Fig.4a (image width: 12.3cm, height: 42.9cm): (a) The enhanced image with phase congruency; (b) the bony features segmentation with the newly developed thresholding strategy; (c) the profile identification of spinous column; (d) the results of spine curvature measurement. The blue line represents the valley bottom in spinous column profile, and red curve is the estimated spine curve with 6th order polynomial fitting to these valley bottoms. The numbers in green and pink text represent tangent at the inflection points and the angle between two adjacent inflections, respectively.

region, $\{[C_{left}^{y}, C_{rig}^{y}\ ], y = 1, \cdots, M\}$, is defined using the outermost points with $PAS(x,y) > T_{Otsu}$ in a row-by-row manner. Moreover, a distance threshold T_{sp} was also used to preserve the continuity of contour. The above rule can be defined using the following equation:

$$\begin{aligned} &PAS(C_{left}^{y}, y) > T_{Otsu}, and\ PAS(x,y) \le T_{Otsu}, x = 1, \cdots, C_{left}^{y} - 1 \\ &PAS(C_{right}^{y}, y) > T_{Otsu}, and\ PAS(x,y) \le T_{Otsu}, x = C_{right}^{y} + 1, \cdots, N \\ &|C_{left}^{y} - C_{left}^{y-1}| < T_{sp}\ and\ |C_{right}^{y} - C_{right}^{y-1}| < T_{sp} \end{aligned} \tag{3}$$

In this study, the threshold T_{sp} was empirically determined from 1 to 10 pixels using training VPI images. The minimum value that can be used for all training images, 5 pixels, was finally selected as the distance thresholds. After the spine contour was segmented from the asymmetry phase map, a polynomial curve fitting was applied to smooth the lateral border lines of spine region (Fig. 4d). With the consideration of the nature of the manual operation in ultrasound scanning, the 9th order, which is 3 higher than the order used for polynomial curve fitting of the spine profile, was empirically selected for smoothing the two border lines in the present study.

As shown in Fig. 4c, the shadows generated by symmetric vertebrae belong to symmetric image features, such as ridges and valleys. The symmetry phase map $PS(x,y)$ was designed to enhance these symmetric bony features, calculated as follows:

$$f_e(x,y) = \begin{cases} PS(x,y) - f(x,y) & x \in [C_{left}^{y}, C_{right}^{y}], y = 1, \cdots, M \\ 0 & \text{otherwise} \end{cases} \tag{4}$$

where $f(x,y)$ denotes the normalized gray-level value at pixel (x,y).The image intensity contrast between the soft tissues and bony features would become higher in the enhanced image. On the basis of the information theory introduced by Shannon [48], the entropy-based thresholding techniques [45] utilize image histogram as a probability distribution to segment the image with maximum information transfer. In this study, the maximum-entropy method [49] was selected to segment the bony features by maximizing the entropy formation between soft tissues and bony features in the spine region. The entropy sum $E(t)$ of the image for sequential values of t can be calculated as:

$$\begin{aligned} E(t) = \ln\{P_1(t)(1 - P_1(t))\} - \left(\sum_{j=0}^{t} p_j \ln p_j\right)/P_1(t) - \\ \left(\sum_{j=t+1}^{K} p_j \ln p_j\right)/(1 - P_1(t)) \end{aligned} \tag{5}$$

where p_j is the image histogram in the spine region, and $P_1(t) = \sum_{j=0}^{t} p_j$. The optimal threshold T_{ME} that maximizes $E(t)$ is the value maximizing the information between the object (i.e., bony features) and the background (i.e., soft tissues) in spine region. The bony features segmentation $B(x,y)$ was then computed as:

$$B(x,y) = \begin{cases} 1 & f_e(x,y) > T_{ME} \\ 0 & \text{otherwise} \end{cases} \tag{6}$$

Fig. 5a and Fig. 5b illustrate the enhanced image and the corresponding bony features segmentation on the VPI image as shown in Fig. 4a, respectively.

C. Identification of Spinous Column Profile

Bony features consist of transverse processes and spinous processes in the spine VPI image. As shown in Fig. 5b, the profile generated by the spinous processes lies in the middle of the image, in which spine curve $S(\boldsymbol{v}) = \psi(x,y)$ in $\mathcal{R}^2$ can be perceived. To achieve the curve detection, a technique for determining the spinous column profile was developed using the segmentation of bony features $B(x,y)$ in a row-by-row manner.

Let $\{[SP_{left}^{k}, SP_{right}^{k}],\ k = 1, \ldots, N_{SP}\}$ denote the detected contour of spinous column profile, and N_{SP} represent the total row number of effective spinous column profile. We briefly describe the procedure used to identify the contour of spinous column profile detection in a sequence of operations:

1) For each row, $y = 1, \cdots, M$, the number of bony segments N_{seg}^{y} was firstly determined by identifying continuous portions from bony features segmentation.
2) When $N_{seg}^{y} \ge 1$, find the segment $[NS_{left}^{y}, NS_{right}^{y}]$ that has the maximum overlapped length with previous spinous profile $[SP_{left}^{prev}, SP_{right}^{prev}]$.
3) Use a distance threshold T_d to check the contour change between the segment $[NS_{left}^{y}, NS_{right}^{y}]$ and the previous spinous profile $[SP_{left}^{prev}, SP_{right}^{prev}]$, avoiding dramatic contour variations.

In our approach, as shown in Fig. 4b, the initial spinous column profile $[SP_{left}^{INI}, SP_{right}^{INI}]$ was estimated using the top contour of spine region obtained from the asymmetry phase measure $PAS(x,y)$. Moreover, the mean width of spinous process has been reported to be about 10 mm [50]. The distance threshold T_d was then empirically determined to be 20 mm, which was about a fifth of the spine region width W_{spine} acquired using a linear ultrasound probe with a field of view of 100 mm. In our experiments, the width of spine region was estimated using the average width of contour $\{[C_{left}^{y}, C_{right}^{y}],\ y = 1, \cdots, M\}$. Fig. 5c shows the example of the spinous column profile detection of the VPI image (Fig. 4a). The details of the spinous column profile detection are summarized in Algorithm

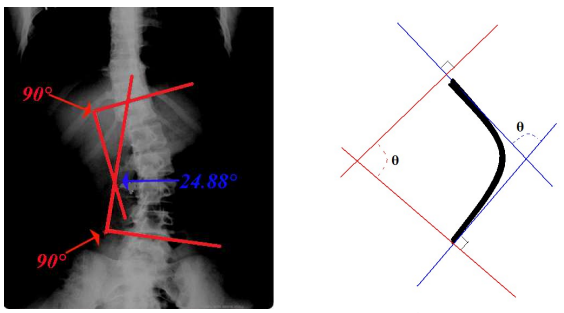

(a) (b)

Fig. 6. The definition of spine curvature angle: (a) The definition of Cobb angle; (b) the definition using the inflection points of curve.

1.

Algorithm 1 Proposed Algorithm for the spinous column profile detection

Initialization: bony features segmentation $B(\mathrm{x},\mathrm{y})$; foreground spine region$\{[C_{left}^{y}, C_{right}^{y}], y = 1, \dots M\}$; $N_{SP} = 0$; $T_d = W_{spine}/5$; $[SP_{left}^{prev}, SP_{right}^{prev}] = [SP_{left}^{INI}, SP_{right}^{INI}]$
Output: The spinous column profile$\{[SP_{left}^{k}, SP_{rig}^{k}\ ], k = 1, \dots, N_{SP}\}$
for y = 1,…,m
  Obtaining the spine region $[C_{left}^{y}, C_{right}^{y}]$
  Deriving the bony features $\boldsymbol{B}(C_{left}^{y}: C_{right}^{y}, y)$ within the spine region
  Identifying the number of bony segments N_{seg}^{y} in the $\boldsymbol{B}(C_{left}^{y}: C_{right}^{y}, y)$
  if $N_{seg}^{y} \geq 1$
    for l = 1,…,N_{seg}^{y}
      Obtaining the overlapped length to previous spinous profile $[SP_{left}^{prev}, SP_{right}^{prev}]$
    end for
    Choosing the segment $[NS_{left}^{y}, NS_{right}^{y}]$ with maximum overlapped length
  else
    continue to next row: $y = y + 1$;
  end if

  if$\{(|NS_{left}^{y} - SP_{left}^{prev}| < T_d)\&\&(|NS_{right}^{y} - SP_{right}^{prev}| < T_d)\}$
    Storing the spinous profile for row:
    $\mathrm{N_{SP}}$+= 1; $\mathrm{SP_{left}^{N_{SP}}} = \mathrm{NS_{left}^{y}}$; $\mathrm{SP_{right}^{N_{SP}}} = \mathrm{NS_{right}^{y}}$;
    $SP_{left}^{prev} = SP_{left}^{N_{SP}}$ and $SP_{right}^{prev} = SP_{right}^{N_{SP}}$
  end if
end for

D. Spine Curvature Measurement

The purpose of spinous column profile detection is to capture valley-like features generated by spinous processes in the spine VPI image. In our approach, we selected the valley bottom of spinous column profile corresponding to the tips of spinous processes as the landmarks to identify the spine curve (Fig. 1). The points with the minimum intensity $\mathrm{S_{cuvre}}(x, \mathrm{y})$ were then located in each row of spinous column profile (Fig. 5c). And a p-th order polynomial curve fitting was applied to the data set $\mathrm{S_{cuvre}}(x, \mathrm{y})$ for obtaining the equation of spine curve $\mathrm{S}(\boldsymbol{v}) = \psi(x, y)$. According to previous studies [51, 52], the 6th order polynomial curve represents the best approximation to the physiological curvature of the spine. The order p was therefore set to be 6 in this study.

Cobb angle is defined as the angle between the lines drawn along the most tilted vertebrae on the radiographs (Fig. 6a), which is actually the angle between the normals to the curves at the corresponding inflection points. As illustrated in Fig. 6b, this definition is the same as that used by the VPI-SP method,

TABLE I
THE PARAMETERS USED IN OUR PROPOSED METHOD

Parameter	Value
Orientations (r)	*6*
Scale (s)	*4*
Wavelength of smallest scale filter	*3*
Scaling factor between successive filter	*2.1*
Ratio of standard deviation to filter center frequency (σ_f/ω_0)	*0.55*
Distance threshold used in spine region (T_{sp})	*5 (pixel)*
Distance threshold used in spinous column profile (T_d)	*20 (mm)*
Polynomial Order in Curve Fitting	*6*

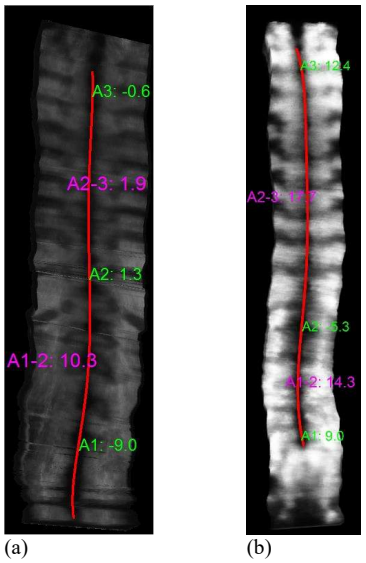

(a) (b)

Fig. 7. The example of spine curvature measurement on VPI images acquired with different gains and probes: (a) The results of VPI image acquired with 100 mm probe and lower gain (image width: 13.5cm, height: 48.0cm); (b) The results of VPI image acquired with 75mm probe and normal gain (image width: 12.0cm, height: 56.2cm). Red curve is the automatically estimated spine curve with 6th order polynomial. The numbers in green and pink text represent tangent at the inflection points and the angle between two adjacent inflections, respectively.

which positions the lines coinciding with tangent lines at the inflection points of curve for curvature measurements. Similarly, in our approach, the spine curvature angle was measured by searching inflection points $\{\boldsymbol{v_i}|\mathrm{S}''(\boldsymbol{v_i}) = 0, \boldsymbol{v}_\mathrm{i} \in f(x, y)$ and $i = 1, \cdots, p-2\}$ to find the maximum angle between the normals of two inflection points. After the inflection points were determined, the angle between two adjacent inflection points was calculated as the corresponding spine curvature angle. Fig.5d presents an example of double curve detection on the image as shown in Fig. 4a.

III. EXPERIMENTS

A total of 70 subjects (age: 15.9 ± 2.7; 22 male and 48 female) were recruited for evaluating the performance of the automatic method for spine curvature assessment. Besides, 29 subjects (age: 30.6 ± 14.7; 9 male and 20 female) reported in our earlier research [29], were also involved in the experiment. Subjects with winged scapula or with BMI higher than 25.0kg/m^2 were excluded. This study was approved by the institutional ethical committee and all subjects gave written informed consent prior to participation in the experiment.

The Scolioscan system (Model SCN801, Telefield Medical Imaging Ltd, Hong Kong), developed based on the 3D ultrasound imaging method as reported in previous studies [16, 22, 23, 26, 29], was used to obtain spine VPI images. Each subject was scanned by the same examiner and volume data was reconstructed for each scan. Based on the collected volumetric data, VPI images were formed by the same examiner, who could select depth and layer thickness for volume projection. Besides the parameters automatically determined in Otsu and the maximum-entropy method, other parameters used in our method, such as those for computing phase congruency, were empirically optimized using training data consisting of 15 VPI

images that were randomly selected from the whole data set. For example, the values used in Kovesi [43] , such as $r = 6$, were eventually selected to compute the phase congruency after evaluating the results of training data. All the recommended values used in this experiment were shown in Table I. Additionally, the values were also validated using VPI images acquired with different gains and probes. As presented in Fig. 7, the spine curves could still be automatically detected using our proposed method with the empirically determined parameters. Furthermore, different values of these empirically optimized parameters only resulted in small boundary variations when spinous column profile could be segmented from the VPI image using these values. For instance, phase congruency calculated with r = 8 and σ_f/ω_0= 0.4 had small boundary differences in spinous column profile in comparison with the result obtained with parameters used in this study (Fig. 8). As illustrated in Fig.1, the detection of the valley bottom in the spinous column profile was hardly influenced by the boundary changes because of the 1-D valley-like curve in each row. The spine curvature measurement obtained using our automatic method was therefore less sensitive to boundary variations of spinous column profile caused by different parameters. The sensitivity analysis of involved parameters used in our method was thus not conducted in the present study.

The VPI-SP and the proposed automatic method were finally used to measure the spine curvature angle in the same VPI image in our experiments. For each VPI image, the spine curvature was measured twice using the VPI-SP method by a single expert who was experienced in ultrasound imaging of scoliosis and blind to the automatic measurement results. The mean value of the manual measurements was used to compare with the automatic measurements. Moreover, the curve number in each image was determined by the same observer, and used for the automatic calculation of spine curvature angle. All measurements of spine curvature were implemented by custom-designed software developed using Visual Studio (Microsoft, Corporation, Washington, USA). As the subjects recruited in the previous study [29] had a large age range (age: 10 ~ 52) in comparison with the newly recruited subjects (age: 8 ~ 23), the experiments were performed on the two datasets separately. The manual measurements of spine curve angle were used as reference and compared with the automatic measurements. A linear regression analysis with zero intercept ($y = kx$; k = regression coefficient) was implemented to describe the relationship between the manual and proposed methods. Pearson product-moment correlations (r) were calculated. Bland and Altman's method of differences [53] was also applied to test the agreement between the two measurements. Level of significance was accepted at $p < 0.05$.

Furthermore, with radiographs provided by their clinicians, 29 subjects who had participated in [29] were also involved in the correlation test between our proposed method and X-ray Cobb's method. The Cobb angle was derived from the radiographs using Cobb's method by software SDV free edition version 1.3 (Santesoft Ltd, Athens, Greece). A linear regression analysis with zero intercept ($y = kx$; k = regression coefficient) was implemented to describe the relationship between the automatic measurement of the ultrasound VPI and the Cobb angle from the radiographs. Pearson product-moment

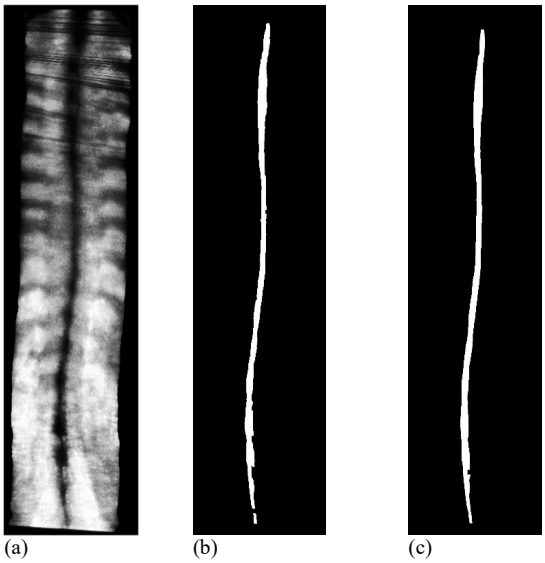

(a) (b) (c)

Fig. 8. An example of spinous column profile identification on VPI image: (a) Original spine VPI image (image width: 12.7cm, height: 50.7cm); (b) the result using phase congruency with r = 6 and σ_f/ω_0 = 0.55; (c) the result using phase congruency with r = 8 and σ_f/ω_0 = 0.4

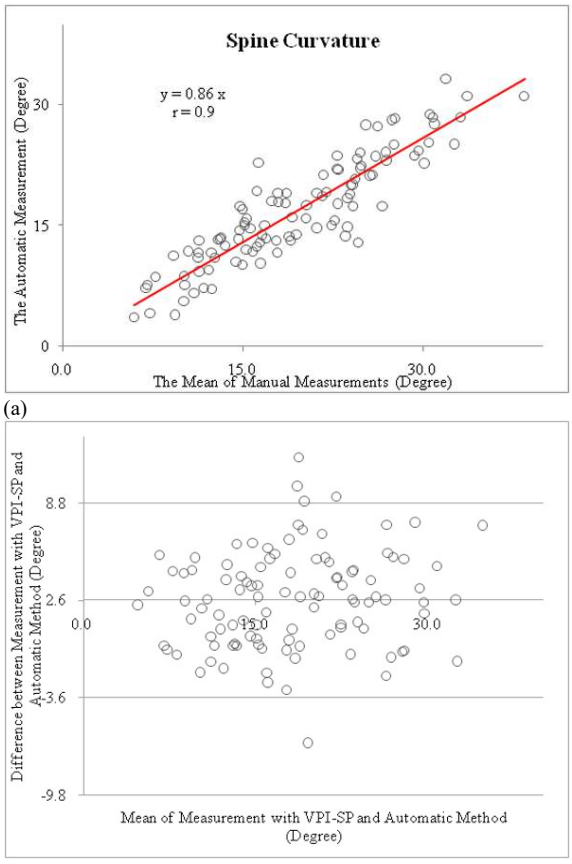

(a)

(b)

Fig. 9. The comparison between the proposed automatic method and VPI-SP for spine curvature assessment in spine VPI images for the newly recruited 70 subjects: (a) The correlation between the angle measured by the proposed automatic method and VPI-SP method; (b) Bland-Altman plot between the angle measured by the proposed automatic method and that by VPI-SP method

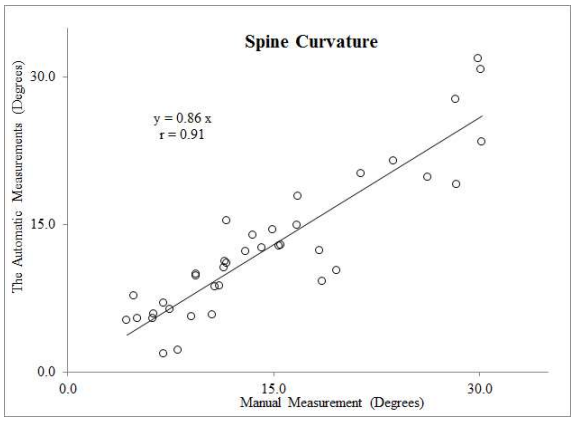

(a)

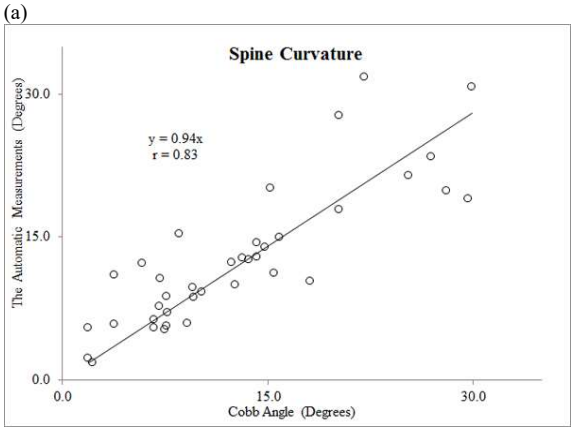

(b)

Fig. 10. The comparison of the proposed automatic method with both Cobb's method and VPI-SP for spine curvature assessment for the subjects presented in [25]: (a) The correlation between the angle measured by the proposed automatic method and VPI-SP method; (b)The correlation between the angle measured by the proposed automatic method and Cobb's method

correlations (r) were calculated. Level of significance was accepted at $p < 0.05$.

IV. Results

For the newly recruited 70 subjects, the spine curvature angle measured by the proposed automatic method ranged from 3.6° to 33.2°, while the angle range using the VPI-SP method was 5.9° to 38.5°. The results revealed a significant linear correlation between the VPI-SP and the automatic method (slope = 0.86, $r = 0.90$, $p < 0.001$, Fig. 9a). As shown in Fig.9b, the Bland-Altman plot between the manual and automatic measurements indicated a low mean difference ($d = 2.6°$) and the symmetrically distributed differences around mean difference were within the limits (±1.96 SD = 6.2°). These results suggested that there was a good agreement between the measurements obtained by the two methods. Moreover, we also compared the automatic measurements with both X-ray Cobb angles and the manual VPI-SP measurements for the data presented in our earlier work [29]. The result obtained using the automatic method had a significant correlation with the measurements by the VPI-SP method (slope = 0.86, $r = 0.90$, $p < 0.001$, Fig. 10a) and X-ray Cobb's method (slope = 0.94, $r = 0.83$, $p < 0.001$, Fig. 10b). These results also demonstrated the feasibility of our proposed method in measuring spine curvature.

Fig. 11 shows an example of the manual and automatic

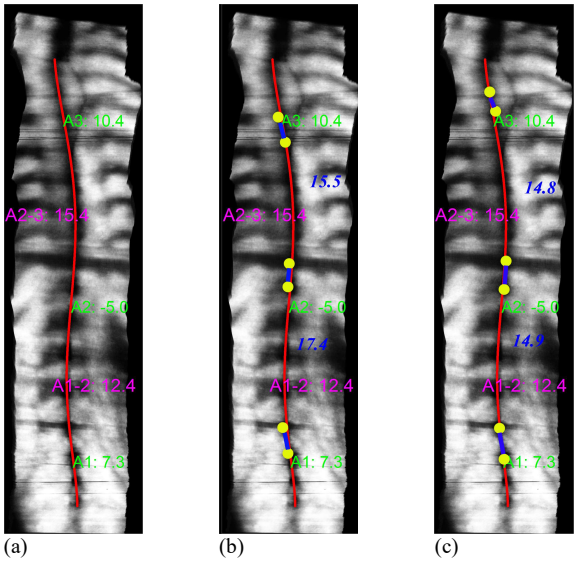

(a) (b) (c)

Fig. 11. An example of spine curvature measurement using the same inflection points between automatic and manual measurements (image width: 12.2cm, height: 47.0cm): (a) The results of our proposed method; (b) the comparison between automatic measurement and the first measurement using VPI-SP method; (c) the comparison between automatic measurement and the second measurement using VPI-SP method. Red curve is the automatically estimated spine curve with 6th order polynomial. The numbers in green and pink text represent tangent at the inflection points and the angle between two adjacent inflections, respectively. Blue lines with yellow dots are the manually identified lines containing inflection points in VPI-SP method. The number in blue text represents the angle between two adjacent drawn lines.

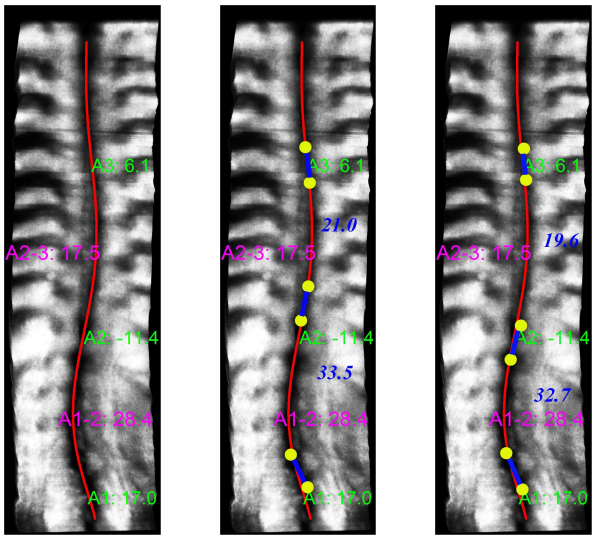

(a) (b) (c)

Fig. 12. An example of spine curvature measurement using different inflection points between automatic and manual measurements (image width: 11.3cm, height: 38.7cm): (a) The results of our proposed method; (b) the comparison between automatic measurement and the first measurement using VPI-SP method; (c) the comparison between automatic measurement and the second measurement using VPI-SP method. Red curve is the automatically estimated spine curve with 6th order polynomial. The numbers in green and pink text represent tangent at the inflection points and the angle between two adjacent inflections, respectively. Blue lines with yellow dots are the manually identified lines containing inflection points in VPI-SP method. The number in blue text represents the angle between two adjacent drawn lines.

measurements of spine curvature angle for one typical subject. As illustrated in Fig. 11b and Fig. 11c, the lines were located almost in the same position for the two manual measurements. It was observed that straight lines identified by the VPI-SP method passed through the points of inflection on the curve obtained using our proposed method. However, the lines could not exactly coincide with the tangent lines at the corresponding inflection points on the curve, thus failing to obtain the same orientation at the inflection points. Moreover, as the lines were manually drawn in the VPI image when using the VPI-SP method, the lines even could not exactly meet with each other between the two measurements for the same VPI image, causing variations in measurements. Fig. 12 shows another example of spine curvature angle measured with the proposed approach, where some of the lines positioned by the VPI-SP method were not in agreement with the inflection points on the curve. Moreover, as shown in Fig. 12b and Fig. 12c, the positions of the lines were also inconsistent between the two manual measurements, contributing to deviations between the measurements. The absolute difference of the manual measurements reached 1.6 ± 1.3° in this study. On the other hand, the automatic method measured the spine curvature according to the inflection points on the spine curve, obviating the variations in measurements. In addition, as illustrated in Fig.13d, Otsu method used in our previous method [33] failed to derive a satisfactory segmentation of spinous column profile from the VPI image, greatly influencing the assessment of spine curvature (Fig. 13a and Fig.13c). By contrast, using the anatomical information of vertebral structures, the spinous column profile segmented with the proposed two-fold thresholding strategy was more consistent with the perception of human vision (Fig. 13b), improving the performance of automatic spine curvature measurement on VPI images. As demonstrated in Fig. 13, the result of our proposed method was closer to the manual value.

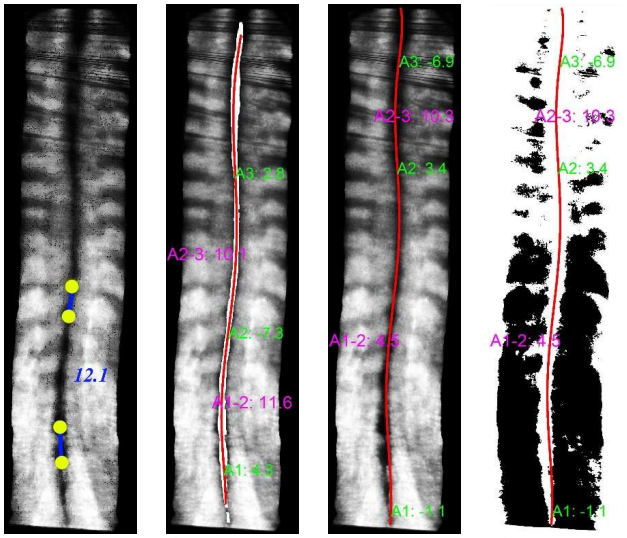

(a) (b) (c) (d)

Fig. 13. An example of spine curvature measurement on the VPI image of Fig.8a using our newly proposed method and the method in [33]: (a) The results using manual VPI-SP method; (b) The curvature measurement and spinous column profile segmentation using our newly proposed method; (c) The curvature measurement using the method in [33]; (d) The OTSU results used by the method in [33]. Red curve is the automatically estimated spine curve with 6th order polynomial. The numbers in green and pink text represent tangent at the inflection points and the angle between two adjacent inflections, respectively. Blue lines with yellow dots are the manually identified lines containing inflection points in VPI-SP method. The number in blue text represents the angle between two adjacent drawn lines.

V. DISCUSSION

We have presented a novel automatic method to measure the spine curvature by utilizing the vertebral anatomical structures in spine VPI image. A newly developed two-fold thresholding strategy was used to separate the symmetric bony features from the preprocessed image using phase congruency. And prior knowledge on the arrangement of VPI images was employed to identify spinous column profile and spine curve. Finally, a 6th order polynomial curve fitting was applied to determine the inflection points of curve for calculating the angle of spine curvature. The feasibility of our proposed method was demonstrated by the significant correlation (slope = 0.86, $r \geq 0.90$, $p < 0.001$) between the results obtained by the manual and automatic methods among 99 subjects with different levels of scoliosis. The results demonstrated that the new measurement method could provide reliable spine curvature measurement with performance comparable to that by the VPI-SP method. Moreover, the high linear correlation between our proposed method and the X-ray Cobb's method among 29 subjects recruited in our earlier work [29] (slope = 0.94, $r = 0.83$, $p < 0.001$) also demonstrated the comparable performance of the new automatic method. We showed that the spine curvature can be assessed automatically in spine anatomy visualization using 3-D ultrasound imaging, eliminating the error in bony features identification and obviating variations in manual measurements. The proposed automatic method could therefore facilitate wide applications of 3-D ultrasound imaging for scoliosis assessment.

The key element in the proposed method is to utilize prior knowledge on vertebral anatomical structures in the ultrasound VPI images. Bones can produce a strong reflection of ultrasound wave, resulting in bony shadow in B-mode images (Fig. 3). The symmetry of vertebral anatomical structures created the symmetric bony shadow in spine VPI images when the average blending function was used in the visualization of spine anatomy. Phase congruency can provide a good measure of symmetric and asymmetric features [35], which is beneficial for feature perception focusing on symmetric structures. As an illumination and contrast invariant measure, symmetry phase measure was employed to enhance the symmetric bony shadow, including spinous column profile and transverse processes, for segmenting the bony features from the VPI image. The prior knowledge of anatomical structures of vertebrae allows for an easier detection of spinous column profile from bony features, as the spinous processes are in the midline of the vertebral body, mainly generating the bony shadow profile in the middle of the VPI image.

The current study employed a 6th order polynomial curve fitting to objectively quantify spine curvature. Both 5th and 6th order polynomial curve fittings have been proposed to quantify scoliotic deformity in previous studies [25, 51, 52, 54]. Nonetheless, it has been suggested that the 6th order polynomial

curve generates the best representation of normal and scoliotic spinal curvature [51, 52]. The Cobb angle obtained by a 6th order polynomial was also reported to be better than that obtained using lower order polynomial [52]. On the other hand, there is lack of reports presenting the spine curve using higher order polynomial, such as 7. The 7th and 8th order polynomial curve fittings were also tried to evaluate the selection of appropriate polynomial order in this study. Preliminary results showed that the differences between using 6th order and other higher orders are very small. Therefore, the 6th order polynomial curve was finally used to fit the spine curve in this study.

The measurement of spine curvature angle using the proposed method *in vivo* showed good agreement with the manual measurement. However, it was found that the results with the proposed method were slightly smaller than those obtained using the VPI-SP method. This could probably be explained by the difference in determining the spine curve, though both methods employed the curve inflection points to measure the curvature. In VPI-SP method, the curve was manually determined based on observations on spinous column profile. It was difficult to make the straight line coincide exactly with the tangent line at the corresponding inflection point (Fig. 11). On the other hand, the spine curve was determined from the valley bottom in spinous column profile, corresponding to the tips of spinous processes, in our proposed method. The automatic method appeared to be more related to the spine curvature, characterizing the spine curve using the tips of spinous processes. In addition, the regression coefficient (slope = 0.91) between the manual and automatic measurements of Cobb angles based on X-ray images in a previous report [52] was a little higher than that in our study (slope = 0.86), though the same 6th order polynomial curve was used to represent the physiological curvature of the spine. This can be attributed to different algorithms used in determining the spine curvature angle. According to the definition in [52], the normals at vertebrae bodies instead of curve inflection points were searched for identifying maximum Cobb angle, resulting in better consistency with the position used in manual measurements. On the other hand, the inflection points were directly applied in the calculation of spine curvature on VPI images. As the inflection point was manually identified in the spine VPI image using the VPI-SP method, the points might be different from the inflection points on the curve obtained by the automatic method proposed in this study, contributing to larger difference in the results between the manual and automatic methods [52].

As a radiation-free imaging modality, the 3-D ultrasound imaging system can be applied for the assessment of scoliosis in teenagers through examining the spine anatomy directly using the spine VPI image [29]. Although the manual measurement using the VPI-SP method had lower intra-observer variations in comparison with X-ray Cobb's method [29], there were always small deviations in the position and orientation of the lines manually identified in the same image among the measurements using VPI-SP method, resulting in variations in measurements (1.6 ± 1.3°). This influenced the sensitivity and specificity of scoliosis diagnosis using freehand 3-D ultrasound imaging system. In addition, measurement time also depended on the experience of the observer in locating the inflection points of curve. The newly proposed method derived the inflection points automatically on the curve according to the tips of spinous processes, avoiding this kind of limitation. Therefore, this new automatic measurement might provide a good method to improve the sensitivity and specificity of scoliosis assessment with 3-D ultrasound imaging system, especially for observing the curve progression and monitoring the treatment outcome of scoliosis. This method might also serve as a good approach to facilitating the application of 3-D ultrasound imaging in mass screening of idiopathic scoliosis, avoiding manual interference and radiation exposure. Further studies are required to demonstrate the feasibility of using the proposed method in diagnosis, treatment, and screening of scoliosis, with a larger group of subjects.

The evaluation using the proposed method could still be affected by several factors. The proposed 3-D ultrasound imaging method measured the spine curvature using the spinous column profile that was different from the bony features used in the X-ray Cobb's method, which uses the plate of vertebra body. This point has been well discussed in earlier studies[16]. In the present study, the proposed method was only compared with X-ray Cobb's method among the 29 subjects presented in our previous work [29], but not for the newly recruited 70 subjects, due to the following factors. 1) Among the subjects newly recruited in this study, some had X-ray examinations taken with their braces while others without. Since ultrasound scanning was conducted without brace, it was not proper to have a direct comparison between Cobb angle and Scolioscan results. 2) The approximate one-month interval between the ultrasound scanning and radiograph examination for some subjects might also affect the comparison because of the curve progression of scoliosis. For those patients with brace treatment completed during the period, the variation might be even larger as there would be some change of curvature after the brace was removed. Scoliosis is recognized as a 3-D spine deformity problem.

In addition, Vertebral rotation is an essential factor for influencing scoliosis 3-D deformity [19], resulting in increasing deviation of spinous processes to the concave side of spine. Herzenberg, et al. [55] reported that the angle using spinous processes underestimated the degree of spine curvature in comparison with the Cobb's method. Although both the manual and automatic measurements using spinous column profile have comparable performance with X-ray Cobb's method for subjects presented in [29], further studies with a large number of subjects should still be conducted to compare the automatic method with Cobb's method under a better control of X-ray and 3-D ultrasound imaging protocols. Moreover, it was assumed that the spinous processes tips were corresponding to the pixel with minimum intensity over the spinous column profile in VPI images. This assumption may not hold in the spinous processes with large deformations and anomalous shapes [29], especially for subjects with high BMI or winged scapula, which increased the difficulty of curve

detection in such cases. In addition, subjects with winged scapula or other irregular back contours might preclude satisfactory skin contact with the probe during scanning. Therefore, ultrasound imaging might fail to depict vertebral anatomical structures in these irregular regions, resulting in invisible spinous column profile in VPI images. This makes it impossible to measure spine curvature using manual or automatic methods on these VPI images; however, the Cobb angle can still be measured on the corresponding X-ray images. Further studies are required to develop a flexible or small probe with good penetration to overcome this limitation of 3-D ultrasound imaging for scoliosis. Furthermore, in the current study, only the measurements on coronal plane was automatically calculated to assess scoliosis. Automatic methods should be extended to other measurements of 3-D spine deformity, such as vertebral rotation, by directly extracting corresponding bony features from 3-D ultrasound data in the future development. Finally, the new method is still a little computationally uneconomic, around 20s for the 600×2000 pixel image using a computer with an Intel Core 2 Q8400 2.66-GHz processor and 2048 MB of memory. The major reason is that the program spent most of the time calculating the phase congruency, which was implemented using log-Gabor wavelet. The computational time can be greatly reduced, since phase congruency calculation can be processed by parallel computation techniques using a Graphics Processing Unit (GPU).

VI. Conclusions

In this paper, a robust automatic algorithm was presented to measure spine curvature in the spine VPI image by utilizing the vertebral anatomical structures with the phase congruency and a newly developed two-fold thresholding strategy. The results showed a good agreement between the automatic and manual measurements and between the automatic results and X-ray Cobb's angle. This method obviated subjective manual measurements, reducing the variations in measurements. We expected that the proposed method would provide an effective way for mass screening idiopathic scoliosis and monitoring curve progression with 3-D ultrasound imaging. Further studies with a large group of subjects would be conducted to demonstrate the potential of this new method for scoliosis diagnosis. The performance of the newly proposed method can be further enhanced by using GPU programming to achieve faster computation in future studies, making it possible to realize fully automatic assessment of scoliosis with a free-hand 3-D ultrasound system and automatic VPI image selection.

Acknowledgments

This study was supported by the Research Grant Council of Hong Kong (PolyU5332/07E, PolyU152220/14E), the Hong Kong Innovation and Technology Fund (UIM213), and the Strategic Important Project of the Hong Kong Polytechnic University (1-ZE23). The authors would like to thank Telefield Medical Imaging Limited for its generous support in providing the Scolioscan system and technical supports for this study. The subjects included in this study were recruited in the Department of Orthopaedics and Traumatology of the Chinese University of Hong Kong, and we would like to thank Prof. Jack Cheng, Dr. Tsz-Ping Lam, and Dr. Bobby Ng and other colleagues for their generous support in subject recruitment. We also thanks Ms Sally Ding for helping us to edit the paper.

Conflict of Interests

The author Zheng YP owned a number of patents related to the Scolioscan system, which have been licensed to Telefield Medical Imaging Limited for commercialization. Zheng YP was currently a consultant for this company for the improvement of Scolioscan system.

References

[1] W. P. Bunnell, "The natural history of idiopathic scoliosis before skeletal maturity.," *Spine,* vol. 11, no. 8, pp. 773-776, 1986.

[2] J. P. Horne, R. Flannery, and S. Usman, "Adolescent Idiopathic Scoliosis: Diagnosis and Management," *American Family Physician,* vol. 89, no. 3, pp. 193-198, Feb, 2014.

[3] M. Konieczny, H. Senyurt, and R. Krauspe, "Epidemiology of adolescent idiopathic scoliosis," *Journal of Children's Orthopaedics,* vol. 7, no. 1, pp. 3-9, 2013/02/01, 2013.

[4] J. Cobb, "Outline for the study of scoliosis. ," *American Academy of Orthopaedic Surgeons Instructional Course Lectures,* vol. 5, pp. 15, 1948.

[5] H. Kim, H. S. Kim, E. S. Moon *et al.*, "Scoliosis Imaging: What Radiologists Should Know," *Radiographics,* vol. 30, no. 7, pp. 1823-1842, Nov, 2010.

[6] R. T. Morrissy, G. S. Goldsmith, E. C. Hall *et al.*, "Measurement of the Cobb angle on radiographs of patients who have scoliosis : evalution of intrinsic error," *Journal of Bone and Joint Surgery-American Volume,* vol. 72A, no. 3, pp. 320-327, Mar, 1990.

[7] D. A. Hoffman, J. E. Lonstein, M. M. Morin *et al.*, "Breast Cancer in Women With Scoliosis Exposed to Multiple Diagnostic X Rays," *Journal of the National Cancer Institute,* vol. 81, no. 17, pp. 1307-1312, Sep, 1989.

[8] A. R. Levy, M. S. Goldberg, N. E. Mayo *et al.*, "Reducing the lifetime risk of cancer from spinal radiographs among people with adolescent idiopathic scoliosis," *Spine,* vol. 21, no. 13, pp. 1540-1547, Jul, 1996.

[9] M. M. Doody, J. E. Lonstein, M. Stovall *et al.*, "Breast cancer mortality after diagnostic radiography - Findings from the US Scoliosis Cohort Study," *Spine,* vol. 25, no. 16, pp. 2052-2063, Aug, 2000.

[10] C. M. Ronckers, M. M. Doody, J. E. Lonstein *et al.*, "Multiple diagnostic x-rays for spine deformities and risk of breast cancer," *Cancer Epidemiology Biomarkers & Prevention,* vol. 17, no. 3, pp. 605-613, Mar, 2008.

[11] D. L. Carman, R. H. Browne, and J. G. Birch, "Measurement of scoliosis and kyphosis radiographs - Intraobserver and interobserver variation," *Journal of Bone and Joint Surgery-American Volume,* vol. 72A, no. 3, pp. 328-333, Mar, 1990.

[12] J. Pruijs, M. Hageman, W. Keessen *et al.*, "Variation in Cobb angle measurements in scoliosis," *Skeletal Radiol,* vol. 23, no. 7, pp. 4, 1994.

[13] M. Wybier, and P. Bossard, "Musculoskeletal imaging in progress: The EOS imaging system," *Joint Bone Spine,* vol. 80, no. 3, pp. 238-243, May, 2013.

[14] S. C. N. Hui, J.-P. Pialasse, J. Y. H. Wong *et al.*, "Radiation dose of digital radiography (DR) versus micro-dose x-ray (EOS) on patients with adolescent idiopathic scoliosis: 2016 SOSORT- IRSSD "John Sevastic Award" Winner in Imaging Research," *Scoliosis and Spinal Disorders,* vol. 11, pp. 46, 2016.

[15] A. Hocquelet, F. Cornelis, A. Jirot *et al.*, "Patient-specific 3D models created by 3D imaging system or bi-planar imaging coupled with Moir,-Fringe projections: a comparative study of accuracy and reliability on spinal curvatures and vertebral rotation data," *European Spine Journal,* vol. 25, no. 10, pp. 3154-3161, Oct, 2016.

[16] Y.-P. Zheng, T. T.-Y. Lee, K. K.-L. Lai *et al.*, "A reliability and validity study for Scolioscan: a radiation-free scoliosis assessment system using 3D ultrasound imaging," *Scoliosis and Spinal Disorders,* vol. 11, no. 1, pp. 1-15, 2016.

[17] R. S. Alomari, S. Ghosh, J. Koh *et al.*, "Vertebral Column Localization, Labeling, and Segmentation," *Spinal Imaging and Image Analysis*, S. Li and J. Yao, eds., pp. 193-229, Cham: Springer International Publishing, 2015.

[18] F. Jager, J. Hornegger, S. Schwab *et al.*, "Computer-Aided Assessment of Anomalies in the Scoliotic Spine in 3-D MRI Images," *Medical Image Computing and Computer-Assisted Intervention - Miccai 2009, Pt Ii, Proceedings*, Lecture Notes in Computer Science G. Z. Yang, D. Hawkes, D. Rueckert *et al.*, eds., pp. 819-826, Berlin: Springer-Verlag Berlin, 2009.

[19] S. Suzuki, T. Yamamuro, J. Shikata *et al.*, "Ultrasound measurement of vertebral rotation in idiopathic scoliosis," *Journal of Bone and Joint Surgery-British Volume,* vol. 71, no. 2, pp. 252-255, Mar, 1989.

[20] K. P. Kennelly, and M. J. Stokes, "Pattern of asymmetry of paraspinal muscle size in adolescent idiopathic scoliosis examined by real-time ultrasound imaging - A preliminary study.," *Spine,* vol. 18, no. 7, pp. 913-917, Jun, 1993.

[21] W. Chen, E. H. M. Lou, and L. H. Le, "Using ultrasound imaging to identify landmarks in vertebra models to assess spinal deformity," *33rd Annual International Conference of the IEEE Engineering in Medicine and Biology Society, EMBS 2011.* pp. 8495-8498.

[22] C. W. J. Cheung, and Y. P. Zheng, "Development of 3-D Ultrasound System for Assessment of Adolescent Idiopathic Scoliosis (AIS)," *6th World Congress of Biomechanics*, IFMBE Proceedings C. T. Lim and J. C. H. Goh, eds., pp. 584-587, New York: Springer, 2010.

[23] C. W. J. Cheung, S. Y. Law, and Y. P. Zheng, "Development of 3-D Ultrasound System for Assessment of Adolescent Idiopathic Scoliosis (AIS) and System Validation," in Engineering in Medicine and Biology Society (EMBC), 2013 35th Annual International Conference of the IEEE, Osaka, Japan, 2013, pp. 6474-6477.

[24] T. Ungi, F. King, M. Kempston *et al.*, "Spinal Curvature Measurement by Tracked Ultrasound Snapshots," *Ultrasound in Medicine & Biology,* vol. 40, no. 2, pp. 447-454, February, 2014.

[25] T. K. Koo, J. Y. Guo, C. Ippolito *et al.*, "Assessment of scoliotic deformity using spinous processes: comparison of different analysis methods of an ultrasonographic system," *Journal of Manipulative and Physiological Therapeutics,* vol. 37, no. 9, pp. 667-677, Nov-Dec, 2014.

[26] C.-W. J. Cheung, G.-Q. Zhou, S.-Y. Law *et al.*, "Freehand three-dimensional ultrasound system for assessment of scoliosis," *Journal of Orthopaedic Translation,* vol. 3, no. 3, pp. 123-133, July, 2015.

[27] K. E. Purnama, M. H. F. Wilkinson, A. G. Veldhuizen *et al.*, "A framework for human spine imaging using a freehand 3D ultrasound system," *Technology and Health Care,* vol. 18, no. 1, pp. 1-17, 2010.

[28] W. Chen, E. M. Lou, P. Zhang *et al.*, "Reliability of assessing the coronal curvature of children with scoliosis by using ultrasound images," *Journal of Children's Orthopaedics,* vol. 7, no. 6, pp. 521-529, 2013/12/01, 2013.

[29] C. W. J. Cheung, G. Q. Zhou, S. Y. Law *et al.*, "Ultrasound Volume Projection Imaging for Assessment of Scoliosis," *IEEE Transactions on Medical Imaging,* vol. 34, no. 8, pp. 1760-1768, 2015.

[30] M. Young, D. L. Hill, R. Zheng *et al.*, "Reliability and accuracy of ultrasound measurements with and without the aid of previous radiographs in adolescent idiopathic scoliosis (AIS)," *European Spine Journal,* vol. 24, no. 7, pp. 1427-1433, Jul, 2015.

[31] Q. N. Vo, E. H. M. Lou, and L. H. Le, "3D ultrasound imaging method to assess the true spinal deformity," *Conference proceedings : ... Annual International Conference of the IEEE Engineering in Medicine and Biology Society. IEEE Engineering in Medicine and Biology Society. Annual Conference,* vol. 2015, pp. 1540-3, 2015, 2015.

[32] B. Lichtenbelt, R. Crane, and S. Naqvi, *Introduction to Volume Rendering*: Prentice Hall PTR, 1998.

[33] G. Q. Zhou, and Y. P. Zheng, "Assessment of Scoliosis Using 3-D Ultrasound Volume Projection Imaging with Automatic Spine Curvature Detection," *2015 IEEE International Ultrasonics Symposium*, IEEE International Ultrasonics Symposium, New York: Ieee, 2015.

[34] N. Otsu, "A Threshold Selection Method from Gray-Level Histograms," *IEEE Transactions on Systems, Man and Cybernetics,* vol. 9, no. 1, pp. 62-66, 1979.

[35] P. Kovesi, "Symmetry and Asymmetry from Local Phase," in Tenth Australian Joint Converence on Artificial Intelligence, 1997, pp. 2-4.

[36] M. C. Morrone, and R. A. Owens, "Feature detection from local energy," *Pattern Recognition Letters,* vol. 6, no. 5, pp. 303-313, Dec, 1987.

[37] I. Hacihaliloglu, R. Abugharbieh, A. J. Hodgson *et al.*, "Bone surface localization in ultrasound using image phase-based features," *Ultrasound in Medicine and Biology,* vol. 35, no. 9, pp. 1475-1487, Sep, 2009.

[38] I. Hacihaliloglu, R. Abugharbieh, A. J. Hodgson *et al.*, "Automatic Bone Localization and Fracture Detection from Volumetric Ultrasound Images Using 3-D Local Phase Features," *Ultrasound in Medicine and Biology,* vol. 38, no. 1, pp. 128-144, Jan, 2012.

[39] I. Hacihaliloglu, A. Rasoulian, R. N. Rohling *et al.*, "Local Phase Tensor Features for 3-D Ultrasound to Statistical Shape plus Pose Spine Model Registration," *IEEE Transactions on Medical Imaging,* vol. 33, no. 11, pp. 2167-2179, Nov, 2014.

[40] I. Hacihaliloglu, P. Guy, A. J. Hodgson *et al.*, "Volume-specific parameter optimization of 3D local phase features for improved extraction of bone surfaces in ultrasound," *International Journal of Medical Robotics and Computer Assisted Surgery,* vol. 10, no. 4, pp. 461-473, Dec, 2014.

[41] E. M. Abu Anas, A. Seitel, A. Rasoulian *et al.*, "Bone enhancement in ultrasound using local spectrum variations for guiding percutaneous scaphoid fracture fixation procedures," *International Journal of Computer Assisted Radiology and Surgery,* vol. 10, no. 6, pp. 959-969, Jun, 2015.

[42] A. Belaid, D. Boukerroui, Y. Maingourd *et al.*, "Phase-Based Level Set Segmentation of Ultrasound Images," *IEEE Transactions on Information Technology in Biomedicine,* vol. 15, no. 1, pp. 138-147, Jan, 2011.

[43] P. Kovesi, "Phase congruency: A low-level image invariant," *Psychological Research-Psychologische Forschung,* vol. 64, no. 2, pp. 136-148, Dec, 2000.

[44] M. Felsberg, and G. Sommer, "The monogenic signal," *IEEE Transactions on Signal Processing,* vol. 49, no. 12, pp. 3136-3144, Dec, 2001.

[45] M. Sezgin, and B. Sankur, "Survey over image thresholding techniques and quantitative performance evaluation," *Journal of Electronic Imaging,* vol. 13, no. 1, pp. 146-168, Jan, 2004.

[46] C.-C. Lai, and D.-C. Tseng, "A Hybrid Approach Using Gaussian Smoothing and Genetic Algorithm for Multilevel Thresholding," *International Journal of Hybrid Intelligent Systems,* vol. 1, no. 3,4, pp. 143-152, 2004.

[47] K. Hammouche, M. Diaf, and P. Siarry, "A comparative study of various meta-heuristic techniques applied to the multilevel thresholding problem," *Engineering Applications of Artificial Intelligence,* vol. 23, no. 5, pp. 676-688, Aug, 2010.

[48] J. C. Russ, *The Image Processing Handbook*, Sixth Edition ed.: CRC Press, 2011.

[49] J. N. Kapur, P. K. Sahoo, and A. K. C. Wong, "A new method for gray-level picture thresholding using the entropy of the histogram," *Computer Vision Graphics and Image Processing,* vol. 29, no. 3, pp. 273-285, 1985.

[50] C. E. W. Aylott, R. Puna, P. A. Robertson *et al.*, "Spinous process morphology: the effect of ageing through adulthood on spinous process size and relationship to sagittal alignment," *European Spine Journal,* vol. 21, no. 5, pp. 1007-1012, May, 2012.

[51] J. Krejci, J. Gallo, P. Stepanik *et al.*, "Optimization of the examination posture in spinal curvature assessment," *Scoliosis,* vol. 7, no. 1, pp. 10, 2012.

[52] T. A. Sardjono, M. H. F. Wilkinson, A. G. Veldhuizen *et al.*, "Automatic Cobb Angle Determination From Radiographic Images," *Spine,* vol. 38, no. 20, pp. E1256-E1262, Sep, 2013.

[53] J. M. Bland, and D. G. Altman, "Statistical methods for assessing agreement between two methods of clinical measurement," *Lancet,* vol. 1, no. 8476, pp. 307-310, Feb, 1986.

[54] D. K. Singh, M. Bailey, and R. Lee, "Biplanar Measurement of Thoracolumbar Curvature in Older Adults Using an Electromagnetic Tracking Device," *Archives of Physical Medicine and Rehabilitation,* vol. 91, no. 1, pp. 137-142, Jan, 2010.

[55] J. E. Herzenberg, N. A. Waanders, R. F. Closkey *et al.*, "Cobb angle versus spinous process angle in adolescent idiopathic scoliosis: The relationship of the anterior and posterior deformities," *Spine,* vol. 15, no. 9, pp. 874-879, Sep, 1990.